STUDY ON PRESSURE CONTROL OF AUTOMATED FIBER PLACEMENT PROCESS

J. F. Li, C. Song, X. F. Wang, J. Xiao*
College of Material Science & Technology, Nanjing University of Aeronautics & Astronautics, Nanjing, China
* Corresponding author (j.xiao@nuaa.edu.cn)

Keywords: *Automated Fiber Placement (AFP), roller, deformation, pressure, pressure control*

1 Introduction

Automated Fiber Placement (AFP) technique is now widely applied to many fields, such as aerospace and military. The automatic process can significantly save labor and reduce material scrap, especially during large-scaled composite components manufacturing. Additionally, it offers the means to form composite products of exceptional quality with higher accuracy and repeatability [1].

Obviously, the processing variables, such as temperature, pressure, rate, can greatly influence the products' properties. Thereby, the parameter control is a critical factor and is worth studying. Compaction pressure is one of the major parameters of a final part quality [2] and the control studies have been conducted by several groups of researchers. A. B. Hulcher et al. [3] performed Optimization studies in with peel specimens. The specimens were fabricated at various compaction loads. The resulting data were fitted with quadratic response surfaces and quantitatively showed that the compaction force affects the quality of the parts significantly. M. Lee [4] studied the pressure with the pneumatic compaction mechanism, and analyzed its possible effect on the composite quality for a towpreg consolidation process. In addition, the accuracy of the compaction force was identified when a pneumatic tool of a robotic machine moving on a rigid worktable. D. H. J. A. Lukaszewicz et al. [5] established process models of mechanical properties of thermoset prepreg in the uncured state for automated layup, and found a simple plastic material law with strain hardening can be used to accurately model the material response under the pressure during automated layup of toughened epoxy prepreg. The purpose of the study was to investigate how the roller pressure affects on the prepreg when laying up and how to manufacture composite products in uniformity by pressure controlling.

2 Analysis of Press Roller

2.1 Theoretical Prediction

The pressure ensures the prepreg tows attached onto the mold or last laminate placed. Since the prepreg tows are deformable while being deposed, the layer thickness differs with the pressure. And problem also exists in the interlaminar properties, under different pressure. For the reasons above, an appropriate and constant pressure is a prerequisite for AFP products of high performance and repeatability.

Usually, the compactor in AFP machine is designed as compaction shoe or compaction roller. In spite of the lower ability to adapt mold surface, the roller structure is simpler and can handle the common fabrication task. To discuss the pressure control problem, the roller's ability to deform should be taken into consideration. If the roller is treated as elastic and the mold surface as rigid, the model can be transferred into an equivalent one of the contact between two elastic cylinders in the same in size and property (see Fig. 1).

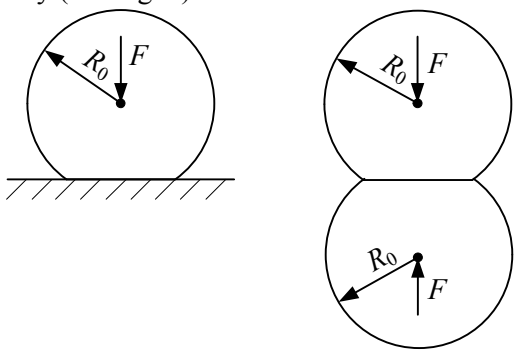

Fig. 1. Equivalent model of the roller deformation

The deformation situation is shown in Fig. 2, when the roller is transferring pressure onto the prepreg tows. The dash lines stand for the contour of roller

(a in length and R_0 in radius) free with press, meanwhile the black lines for the deformed one. Assuming that the deformation d is relatively small, then $q(x)$ represents for the linear force distributed along the width $2b$ in contact surface, whose average value is q_0. And the distributed forces are statistically equivalent to the concentrated force F. Assuming that the elastic modulus is E and the Poisson's ratio is ν associated with the roller material, the problem can be solved, according to the classical solution for non-adhesive elastic contact [6] (see Appendix A). The pressure is variably distributed on the contact area, and the maximum compressive stress occurs at the middle point. Therefore, the following equations can be obtained:

$$q(x)=\frac{2F\sqrt{b^2-x^2}}{\pi ab^2} \tag{1}$$

$$k=\frac{1-\nu^2}{E} \tag{2}$$

$$b=\sqrt{\frac{4R_0k}{\pi}\frac{F}{2ab}} \tag{3}$$

Given the geometric condition

$$\left(R_0-d\right)^2+b^2=R_0^2 \tag{4}$$

If the force is considered uniformly distributed along the length a in contact surface, regardless of the boundaries. Then the force

$$F=2q_0b=\frac{\pi a\left(2R_0d-d^2\right)}{4kR_0} \tag{5}$$

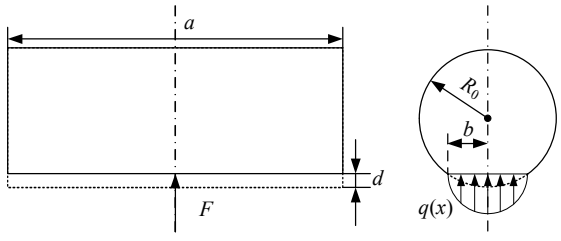

Fig. 2. Schematic diagram for deformed roller

2.2 Finite Element Analysis

To simulate the situation more accurately, a finite element analysis has been conducted by ABAQUS®. The material of roller axis is defined as steel, and the roller rubber. The mechanical property of rubber is hyperelastic, and applied is the Mooney-Rivlin model, which is a classical one for rubber. The elastic constants are determined by the stress–strain data of uniaxial test, achieved by rubber compression experiment. In accordance with the theoretical prediction, the mold is set as an analytic rigid shell. To improve the simulation efficiency, the roller and its axis are assigned by CPS4R elements within reduced integration. To investigate the roller deformation-force relationship, the applied force is set in different values (50 *N*, 100 *N*, 150 *N*, 200 *N*, 250 *N*, 300 *N*, 350 *N*, and 400 *N*), and the deformation can be measured by the displacement of the node on the axis.

Fig. 3 shows the stress distribution of the roller by the software. And the maximum compressive stress appears in the middle of the contact region, which is consistent with the theoretical analysis in Section 2.1.

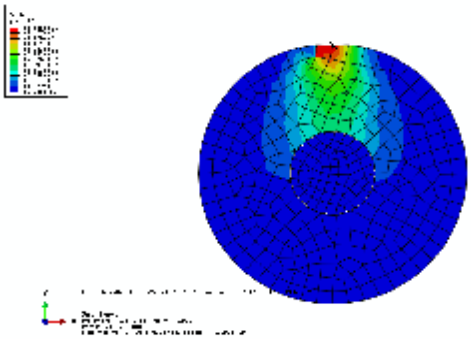

Fig. 3. Stress distribution of the roller by simulation

According to Equation (5), the simulating results are fitted into curve with the application of MATLAB™. The result shows that the curve can fit the simulation data well, if k =0.390 mm^2/N. To present a sensitivity analysis, utilized are the mean-square error (MSE) and mean absolute percentage error (MAPE), based on the calculation. The equations are presented as follows:

$$\mathrm{MSE}=\frac{\sum_{i=1}^{n}\left(\mathrm{Act}_i-\mathrm{Fit}_i\right)^2}{n} \tag{6}$$

$$\mathrm{MAPE}=\frac{1}{n}\left(\left(\sum_{i=1}^{n}\frac{\left|\mathrm{Act}_i-\mathrm{Fit}_i\right|}{\mathrm{Act}_i}\right)*100\%\right) \tag{7}$$

Here, Act_i and Fit_i stands for actual output (the simulated values) and forecasting output respectively. The analysis reveals that the MSE is 453.090 and the MAPE is 12.96%. And the simulation result shows the predicted tendency approximately.

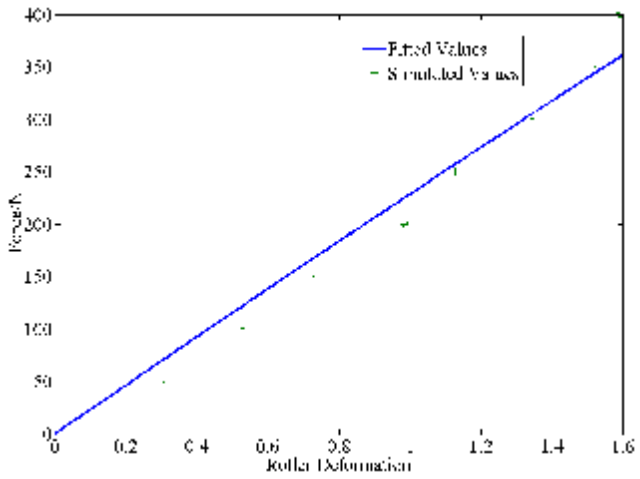

Fig. 4. Curve fitting of roller deformation and force by ABAQUS® simulation

3 Experiments and results

3.1 Experiments

In order to validate the theoretical prediction and finite element analysis, experiments were conducted by a CMT5105 materials testing machine (producer: MTS-SANS). Fig. 5 shows the roller deformation testing device measuring displacement and load. The max load value was set as around 400N, in prevention of failure.

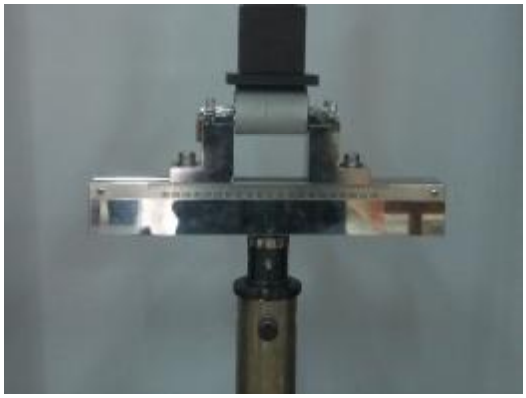

Fig. 5. Roller deformation testing device

The load value and the displacement represent the pressing force on the roller and the deformation amount respectively. The results demonstrated that F escalates as d increases, in coincidence with the prediction and analysis.

3.2 Curve Fitting

For the applying of preload, an initial displacement d_0 should be taken into account. Then Equation (5) can be rewritten into:

$$F = \frac{\pi a E}{4R_0\left(1-\nu^2\right)}\left(2R_0\left(d_0+d\right)-\left(d_0+d\right)^2\right) \qquad (8)$$

According to Equation (8), the curve fitting was completed by MATLAB™ as shown in Fig. 6. And the actual values can be precisely fitted, when k =0.349 mm^2/N and d_0 =0.2105 mm. According to the analysis, the MSE is 53.153 and the MAPE is 3.88%, which indicates the forecast is valid enough.

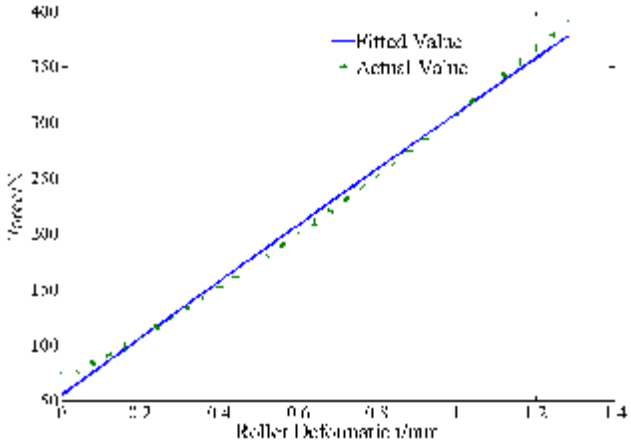

Fig. 6. Curve fitting of relationship between roller deformation and force

Therefore, the application of classical solution can be valid enough to figure out the roller deformation problem.

Given the typical Poisson's ratio of rubber ν =0.475, the elastic modulus can be estimated as 2.22 *MPa*. And this value can be used to check the result of the curve fitting. According to the linear elastic indentation hardness, a relation between the *ASTM D2240* [7] hardness and the Young's modulus for elastomer, derived by Gent [8] and by Mix and Giacomin [9], the relationship

$$E = \frac{0.0981\left(56+7.62336S\right)}{0.137505\left(254-2.54S\right)} \qquad (9)$$

where E is the Young's modulus in *MPa* and S is the *ASTM D2240* [7] type A hardness.

Also another relation that fits the experimental data slightly better is [10]

$$S = 100\,\mathrm{erf}\left(3.186\times10^{-4}E^{1/2}\right) \qquad (10)$$

where erf is the error function and E is in units of *Pa*. Therefore, the hardness are 47.3 *HA* and 49.8 *HA* by the calculations respectively. After measuring the roller rubber material with a Shore durometer, the real hardness is 50.0 *HA*, which is very close to the predicted values. Therefore, relationship gained

from the theoretical prediction (Section 2.1) is proved to be valid enough.

With the acquisition of k and d_0, the relationship between the force and pressure can be predicted, and thus being applied to control the pressure and to predict the quality.

4 Pressure Effect

4.1 Adhesive Patch Growth

The roller pressure exists during the lay-up process, since it drives the prepreg tows onto the substrate. The contact between prepreg and substrate influence the adhesion directly. Therefore, the mechanics of the adhesive contact should be studied.

Gutowski and Bonhomme considered only a very small portion of the available area actually establishes contact. However, the area can hold the prepreg in place and maintain its conformance to the substrate. The resin is described to behave as a Newtonian fluid, and the problem is derived to be a situation which gives the parabolic pressure profile for the circular geometry. Through these assumptions, adequately developed were mathematical models of the adhesive patch growth [11].

In order to examine the pressure effect, the problem can be regarded as squeezing flow between two parallel disks (see Fig. 7) [12]. The disks are separated by a gap with a distance $2h(t)$, which is variable during the patch growth. Assuming that the resin patch is in the form of cylinder similarly, its length is $2h(t)$ and radius is $R(t)$, which is variable as well. The resin's Newtonian viscosity is μ, and the pressure is p_b at the boundary. Moreover, the roller's parameters are set consistent with the former assumption in the theoretical analysis.

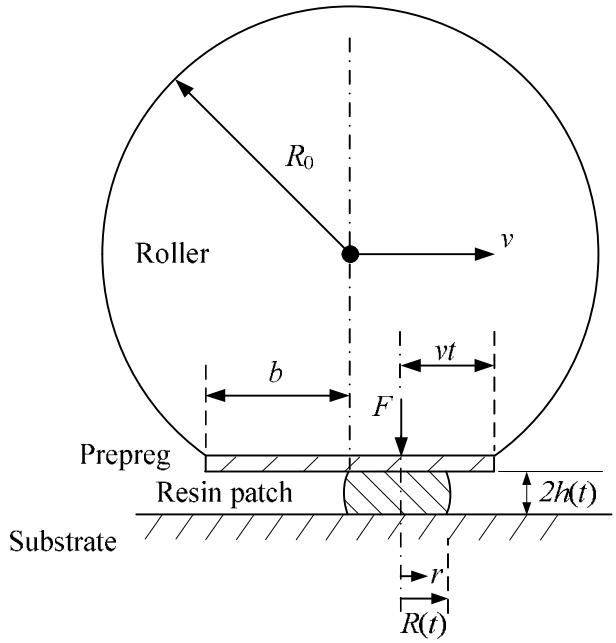

Fig. 7. Geometry for the squeezing flow between two parallel disks for patch growth under roller pressure

Therefore, the resin pressure $p(t)$ at the point, which is r in distance to the patch's centerline, meets the equation (see Appendix B):

$$p(t)-p_b=\frac{3(-h')\mu R^2(t)}{4h^3}\left[1-\left(\frac{r}{R(t)}\right)^2\right] \tag{11}$$

Here h' stands for dh/dt. To simplify the problem, p_b can be approximately considered as 0 and the resin pressure balance with the applied force F_a on the patch area generated by the roller. Then obtained can be the equation showing the pressure balance at the height of ($z=h(t)$).

$$\begin{aligned} F_a &= \int_0^{2\pi}\int_0^{R(t)}\left(p(t)-p_b\right)\Big|_{z=h(t)} rdrd\theta \\ &= \frac{3\pi R^4(t)\mu(-h')}{8h^3(t)} \end{aligned} \tag{12}$$

If the area of contact region is $A(t)=\pi R^2(t)$, and the volume of the patch $V=2h(t)A(t)$ is constant, Equation (12) can be rewritten.

$$F_a=-\frac{3\mu}{32\pi}V^2\frac{h'}{h^5(t)} \tag{13}$$

If the variation of the F_a is taken into account, the applied force $F_a = qA = q\pi R^2(t)$. Furthermore, q can be rewritten into the function of time t.

$$q = q(vt) = \frac{2F\sqrt{b^2 - (b - vt)^2}}{\pi a b^2} \tag{14}$$

Here, v stands for the moving velocity of roller, i. e. the placement rate. Then

$$\frac{2F}{ab^2}\sqrt{b^2 - (b - vt)^2}R^2(t) = -\frac{3\mu}{32\pi}V^2\frac{h'}{h^5(t)} \tag{15}$$

This equation should be rewritten to show the force-time superposition.

$$\frac{2F}{ab^2}\int_{t_1}^{t_2}\sqrt{b^2 - (b - vt)^2}\,dt = -\frac{3\mu}{16}V\int_{h_1}^{h_2}h^{-4}dh \tag{16}$$

To study the adhesive patch growth during the roller pressing period, the total time is $T_t = 2b/v$. For $t_1 = 0$, $t_2 = T$, $h_1 = h(0)$ and $h_2 = h(T_t)$, the following relationship can be obtained.

$$\frac{A(T_t)}{A(0)} = \frac{h(0)}{h(T_t)} = \left[1 + \frac{16\pi F h^2(0)}{\mu a v A(0)}\right]^{\frac{1}{3}} \tag{17}$$

$A(T_t)$ stands for the area of resin patch after applying roller pressure, and its value can be treated as a measure of placement quality.

Therefore, several factors can be observed from Equation (17). The applied force F on the roller contributes to the prepreg adhesion directly. And the growing resin patch area tends to be larger, while lowering the Newtonian viscosity of the resin μ, the roller length a and the placement rate v. However, the width $2b$ of the contact surface which is affect by the elastic modulus E and the Poisson's ratio ν, shows no relationship with $A(T_t)$. Thus, made can be the conclusion that the roller materials have little influence on the processing quality, in the situation of small roller deformation.

For the relationship between Newtonian viscosity and temperature, the temperature is a significant factor to the patch growth. For polymer melts or other fluids, the Williams-Landel-Ferry model [13], or WLF for short, is usually used that have a glass transition temperature. For thermoset prepreg lay-up, the WLF equation, an empirical equation associated, can be applied.

$$\mu(T) = \mu_0 \exp\left(\frac{-C_1(T - T_r)}{C_2 + T - T_r}\right) \tag{18}$$

where T stands for temperature, C_1, C_2, T_r and μ_0 are empiric parameters. Only three of the four constants are independent from each other. To select the parameters, T_r can be based on the glass transition temperature, then C_1 and C_2 may become very similar for the wide class of polymers, prepreg resin included. Also, there are some other suggestions about the parameter selection [14]. However, C_1 and C_2 are supposed to be negative constants, since typical processing temperature T is lower than glass transition temperature, for thermoset prepreg lay-up. The viscosity $\mu(T)$ decreases when the temperature goes up, which can be concluded from Equation (18). As a result, the higher temperature in normal range (be) can accelerate the patch growth, by which can better improve the forming quality.

4.2 Pressure Orientation

To keep the different parts within similar property in the same component, the prepreg tows should be laid under the same circumstance. Indicated from the former study, the applied force is a direct factor count on roller pressure. Therefore, maintained in stably should be the pressing force by the end-effector (AFP head).

However, the complex surfaces often make it difficult to realize during high-speed processing due to the possible diversity of pressure orientations. Fig. 8 shows two different poses (positions and orientations) of AFP head. The force of first AFP head is parallel to the normal (dot-dashed line) of placing point in the surface. Compared to former situation, in the second pose, AFP head has an angle θ between the normal of the placing point and the force direction. Assuming that the original applied force in the AFP head is both F_0, the force values transferred onto the prepreg are $F_1 = F_0$ and $F_2 = F_0\cos\alpha$ respectively. The different force values on the tows can cause the variable forming quality within different areas. Therefore, the end-effector should keep parallel to the normal of the processing point anywhere on the mold surface. Moreover, this orientation guarantees the force to

effect maximally, through transmitting all the force onto the prepreg material.

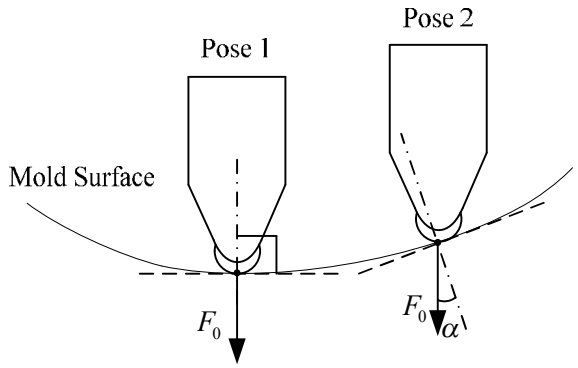

Fig. 8. AFP head poses on mold surface during processing

4.3 Pressure Maintenance

Not only the poses should be taken into account, but the pressure should be also hold in constancy. And the methods for AFP head design should be proposed to deal with the problem. Although the structure of AFP head can be diverse and complicated, the pressure usually originates from the cylinders assembled in AFP head, as simply illustrated in Fig. 9. Since the existence of the movable part, its weight will affect the pressure during processing. The pressing force F of the roller can be expressed as $F = F_C + w_M \cos\varphi$, if introduced were the force F_C provided by cylinder(s), the weight w_M of the movable part and the angle φ between pressing orientation and the gravity direction. For the possible poses of AFP head, solutions should be promoted to achieve a constant pressure.

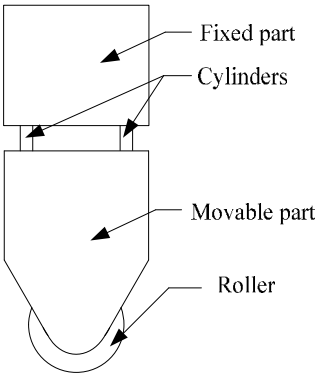

Fig. 9. Schematic diagram for an AFP head structure

1) By simplifying its structure or mounting the attachments to fixed part, minimized can be w_M and its influence on F .

2) Another way is changing F_C by adjusting the air pressure of cylinder(s), in accordance of the φ value.

$$p_C = \frac{F_C}{S} == \frac{F - w_M \cos\varphi}{S} \tag{19}$$

Here, p_C stands for the air pressure in cylinder(s) and S for bore area of the cylinder(s).

3) To eliminate the effect of w_M , assembled can be a balancing structure whose weight $w_B = w_M$. Employed by a pulley device, w_B can be transferred into a pulling force on the movable part, and cause the pressing force in constancy.

$$F = F_C + w_M \cos\varphi - w_B \cos\varphi = F_C \tag{20}$$

Compared to the first solution, the last can completely void the effect of w_M . Additionally, unlike the second one, the goal can be achieved by reasonable design in Solution 3 without complicated control scheme of the cylinder(s). In conclusion, the last solution can be a simple and novel way to solve the pressure variation caused by the weight of movable part of AFP head.

5 Summary

The above tasks have been accomplished to settle the essential problem of AFP pressure control. The roller deformation was both investigated by theoretical analysis and simulation, which were later on validated by experiments. Additionally, being considered as squeezing flow between two parallel disks, the prepreg patch growth under roller pressure was modeled. Investigated was the relationship between the lay-up quality and the processing parameters, especially roller pressure. It was concluded that the force has a pivotal effect on the prepreg conformance, when the roller deformation is relatively small. Moreover, larger roller length or placement rate lead to worse laying quality shows,. On the contrary, the higher temperature offers the process a more suitable environment. Unexpectedly, the roller material is not a factor. the pressure maintenance problem was described in detail. And its solutions were put forward as well, in order to keep a stable pressure.

Appendix A

The two long contacting cylinders (a in length and R_0 in radius) with parallel axes, are pressed against each other by F [15]. Two points, P_1 and P_2 on the surfaces of cylinders, are a distance x from a plane passing through the axes of the cylinders (Fig. 1A). The distance between these points before deformation, $2y$ can be calculated, approximately.

$$2y \cong x^2/R_0 \tag{A1}$$

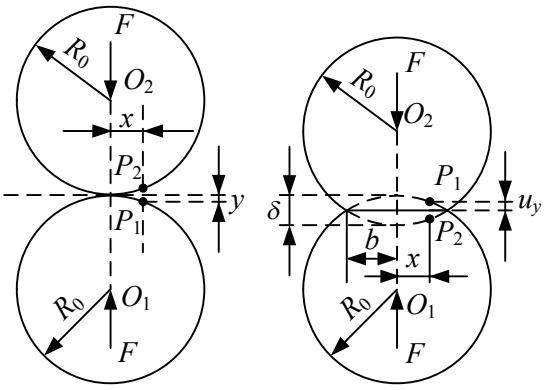

Fig. A1. Contact of two long cylinders with parallel axes

Assuming that the cylinders are flattened in the region, forming a plane of contact in the shape of a straight strip of width $2b$ and of length a, and their axes come closer together by δ.

If the deformation is small ($b \gg x$), the points P_1 and P_2 will coincide.

$$\delta - 2u_y = 2y \tag{A2}$$

Here, u_y represents the vertical projections of the displacements of the points, P_1 and P_2.

If the pressure on the contact area is variable, the following relationship can be obtained

$$\int_{-b}^{b} q(\xi)d\xi = F/a \tag{A3}$$

The load $q(\xi)$ is the applied force per unit width $d\xi$.

If the width of the plane of contact is relatively small compared to R_0, the cylinders can be approximately seen as elastic half-plates. Combining with Flamant's formula [16], obtained may be the displacement of P_1 in the vertical direction under the load $q(\xi)$ acts on a strip of width $d\xi$.

$$du_y = -\frac{2(1-\nu^2)}{\pi E}\left[\ln|x-\xi| + \frac{1}{2(1-\nu)} - \ln R_0\right] q(\xi)d\xi \tag{A4}$$

Then, the total displacement u_y can be integrated from Equation (A4).

$$u_y = -\frac{2(1-\nu^2)}{\pi E}\left\{\int_{-b}^{b} q(\xi)\ln|x-\xi|d\xi + \left[\frac{1}{2(1-\nu)} - \ln R_0\right]q\right\} \tag{A5}$$

Through Equation (A1), (A2) and (A5), we find

$$\frac{4(1-\nu^2)}{\pi E}\int_{-b}^{b} q(\xi)\ln|x-\xi|d\xi = \frac{1}{R_0}x^2 + C \tag{A6}$$

In this equation, C stands for the sum of terms independent of x.

By differentiating with respect to x, and eliminating the integration $x-\varepsilon_1 < \xi < x+\varepsilon_2$, when ε_1 and ε_2 tend to zero, $\lim(\varepsilon_2/\varepsilon_1) = 1$, and the integrand tends to infinity [17], we can obtain an integral equation of the form

$$\frac{4(1-\nu^2)}{\pi E}\int_{-b}^{b} \frac{q(\xi)}{x-\xi}d\xi = \frac{2}{R_0}x \tag{A7}$$

By solving equation (A7), the following expression of $q(x)$ can be achieved.

$$q(x) = \frac{q_{\max}}{b}\sqrt{b^2 - x^2} \tag{A8}$$

Here $q_{\max} = 2F/\pi ab$ and $b = \sqrt{4FR_0(1-\nu^2)/\pi aE}$. The maximum compressive stress $q_{\max}$ occurs at the middle of the strip of contact.

Appendix B

By introducing a cylindrical coordinate system with z-axis coinciding with the symmetry axis of the flow, the two disks defined by z=-h(t) and z=h(t). Since the small gap distance h<<R, the primary flow will be in the r-direction, i. e. v_z<<v_r and $(\partial v_r/\partial r) \ll (\partial v_r/\partial z)$. According to the quasi-steady-state approximation, it can be taken that $\rho\partial v_r/\partial t \ll \mu\partial^2 v_r/\partial z^2$. Therefore, the equation of continuity

$$\frac{1}{r}\frac{\partial}{\partial r}(rv_r) + \frac{\partial v_z}{\partial z} = 0 \tag{B1}$$

the *r*-component of the equation of motion

$$0 = \frac{\partial p}{\partial r} + \mu \frac{\partial^2 v_r}{\partial z^2} \quad \text{(B2)}$$

and the *z*-component of the equation of motion

$$0 = -\frac{\partial p}{\partial z} \quad \text{(B3)}$$

Since the velocity field has the form $v_r = v_r(r,z,t)$ and $v_z = v_z(z,t)$, it can be set that $v_r = rf(z,t)$ in the demands of continuity equation. And the two equations of motion imply that p has the form $p = p_0 + p_2 r^2$, in which p_0 and p_2 are constants. Moreover, these boundary conditions should be satisfied:

$$\partial f / \partial z = 0 \text{, at } z = 0 \quad \text{(B4)}$$

$$f = 0 \text{, at } z = h \quad \text{(B5)}$$

$$v_z = 0 \text{, at } z = 0 \quad \text{(B6)}$$

$$v_z = h' \text{, at } z = h \quad \text{(B7)}$$

$$p = p_b \text{, at } r = R \quad \text{(B8)}$$

Here h' stands for dh/dt, and p_b is the pressure at the boundary. The results are solved by these equations:

$$v_r = \frac{3}{4}\frac{(-h')}{h} r \left[1 - \left(\frac{z}{h}\right)^2\right] \quad \text{(B9)}$$

$$v_z = \frac{3}{2} h' r \left[\frac{(z)}{h} - \frac{1}{3}\left(\frac{z}{h}\right)^3\right] \quad \text{(B10)}$$

$$p - p_b = \frac{3(-h')\mu R^2}{4h^3}\left[1 - \left(\frac{r}{R}\right)^2\right] \quad \text{(B11)}$$

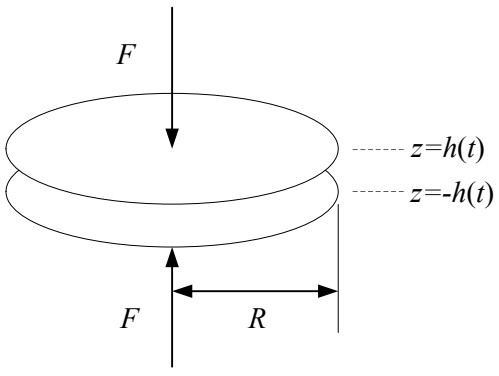

Fig. B1. Squeezing flow between parallel disks

References

[1] G. Marsh "Automating aerospace composites production with fibre placement". *Reinforced Plastics*, Vol. 55, No. 3, pp 3732-3737, 2011.

[2] K. D. Felderhoff, K. V. Steiner "A new compact robotic head for thermoplastic fiber placement". *38th International SAMPE Symposium and Exhibition: Advanced Materials: Performance Through Technology Insertion*, Anaheim, pp 138 -151, 1993.

[3] A. B. Hulcher, W. I. Banks, R. B. Pipes, et al. "Automated fiber placement of PEEK/IM7 composites with film 120 interleaf layers". *46th International SAMPE Symposium and Exhibition: A Materials and Processes Odyssey*, Vol. 46, pp 1998-2012, 2001.

[4] M. Lee. "Heat transfer and consolidation modeling of composite fiber tow in fiber placement". Blacksburg: Virginia Polytechnic Institute & State University, 2004.

[5] D. H. J. A. Lukaszewicz, K. Potter "Through-thickness compression response of uncured prepreg during manufacture by automated layup". *Proceedings of the Institution of Mechanical Engineers Part B-Journal of Engineering Manufacture*, Vol. 226, No. B2, pp 193-202, 2012.

[6] H. R. Hertz "*On the contact of rigid elastic solids and on hardness, Chapter 6*". Macmillan, 1882.

[7] American Society for Testing and Materials "*ASTM D 2240-97, Annual Book of American Society for Testing and Materials Standards*". American Society for Testing and Materials, 1997.

[8] A. N. Gent "On the relation between indentation hardness and Young's modulus". *Rubber Chemistry and Technology*, Vol. 34, No. 4, pp 896-906, 1958.

[9] A. W. Mix and A. J. Giacomin "Standardized polymer durometry". *Journal of Testing and Evaluation*, Vol. 39, No. 4, pp 1-10, 2011.

[10] British Standards Institution "*Chemical tests for raw and vulcanized rubber*". British Standards Institution, 1994.

[11] T. G. Gutowski and L. Bonhomme "The mechanics of prepreg conformance". *Journal of Composite Materials*, Vol. 22, No. 3, pp 204-223, 1988.

[12] R. B. Bird, R. C. Armstrong and O. Hassager "*Dynamics of Polymeric Liquids, Fluid Mechanics*". 2nd edition, John Wiley &Sons, 1987.

[13] M. L. Williams, R. F. Landel, and J. D. Ferry "The temperature dependence of relaxation mechanisms in amorphous polymers and other glass-forming liquids". *Journal of American Chemistry Society*, Vol. 77, No. 14, pp 3701-3707, 1955.

[14] D. W. van Krevelen and P. J. Hoftyzer "Newtonian shear viscosity of polymeric melts". *Die Angewandte*

Makromolekulare Chemie, Vol. 52, No. 1, pp 101–109, 1976.

[15] V. G. Rekach "*Manual of the theory of elasticity*". Mir Publishers, 1979.

[16] M. Flamant "Sur la répartition des pressions dans un solide rectangulaire chargé transversalement". *Comptes Rendus Hebdomadaires de Séances de l'Académie des Science*, Vol. 114, pp 1465–1468，1892.

[17] Z. Tadmore and C. G. Gogos "*Principles of Polymer Processing*". 2nd edition, John Wiley &Sons, 2006.